

## Steric Isotope Effects Gauged by the Bowl-Inversion Barrier in Selectively Deuterated Pentaarylc corannulenes

Tomoharu Hayama, Kim K. Baldridge,\* Yao-Ting Wu, Anthony Linden, and Jay S. Siegel\*

*Institute of Organic Chemistry, University of Zurich, Winterthurerstrasse 190, CH-8057 Zurich, Switzerland*

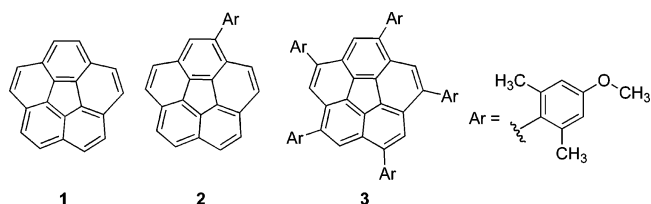
Received May 13, 2007; E-mail: jss@oci.unizh.ch

**Abstract:** Motivated by a greater bowl depth and barrier to bowl inversion in *sym*-1,3,5,7,9-pentamansylcorannulene compared to corannulene, an experimental plan is developed to measure the effective hydrogen/deuterium steric kinetic isotope effect (KIE). Symmetry arguments are used to design orthogonal isotope labeling patterns so that the barrier for the CD<sub>3</sub> compound can be measured in the presence of the CH<sub>3</sub> compound. This scheme eliminates the differential uncertainty in the temperature measurement by allowing both barriers to be measured in the same sample, which in turn reduces the error in determining the differential barrier. Ab initio computations corroborate the structure and isotope effect found experimentally. The predicted and determined steric KIE at 250 K is 1.08 (modified QUIVER at M06-2X/cc-pVDZ) and  $1.22 \pm 0.06$  (VT-NMR), respectively. The results stem from differences in zero-point energy of the CH and CD motions; however, the phenomenology makes the CD<sub>3</sub> group appear effectively “stickier” than CH<sub>3</sub>. The more the C–H···X interaction steepens the well, the “stickier” C–D should appear to be relative to C–H—an important consideration for molecular recognition and one supported by stronger binding constants for deuterated substrates.

### Introduction

Systematic study of the differences in bowl-inversion barriers among corannulene (**1**) and derivatives can serve as a way to gauge steric or electronic aspects of molecular recognition normally dealt with in supramolecular chemistry.<sup>1</sup> The first indication that transannulene interactions of substituents might play a role in the bowl-inversion process came about shortly after observing a relationship of bowl depth to bowl inversion using a structure–energy correlation analysis, à la Bürgi and Dunitz.<sup>2</sup> The bowl-inversion barrier for a series of corannulene derivatives was determined by dynamic variable temperature NMR (DNMR) techniques and a correlation emerged ( $E_a = Cx^4$ ) wherein a deeper bowl depth ( $x$ ) gave rise to a higher inversion barrier ( $E_a$ ). In general, increasing alkyl substitution on the rim leads to a shallower bowl and lower barrier. This correlation holds also for monoaryl derivatives of corannulene like mansylcorannulene (**2**); however, *sym*-pentamansylcorannulene<sup>3</sup> (**3**), a compound with a crown of methyl groups around the rim of the bowl, showed an anomalously high barrier. Quantum mechanical calculations suggested that van der Waals (vdW) attractive forces among the *endo* methyl groups in **3** could contribute to this unusual dynamic behavior.<sup>4</sup> This hypothesis

suggested the possibility to predict and measure the relative attractive steric isotope effect using selectively deuterated derivatives of **3**.<sup>5</sup>



**Indications of a van der Waals Stabilizing Effect.** Agreement between the computational structure of *sym*-penta(2,6-dimethylphenyl)corannulene (**4**) and the X-ray crystallographic structure of **3**<sup>6</sup> was initially investigated. On the basis of previous computational studies, B3LYP/cc-pVDZ was chosen as the initial level for modeling of **4**. Computation of **4** at this level predicts a classical 5-fold symmetric bowl form with the dimethylphenyl rings twisted with respect to the rim of the corannulene placing one methyl group inside the bowl (Me<sub>(endo)</sub>) and one outside (Me<sub>(exo)</sub>). The bowl is predicted to be slightly shallower than **1** (depth<sub>hub-to-rim</sub> = 0.854 Å calcd vs depth 0.873 Å calcd). This simple structural parameter in combination with the above-mentioned structure–energy correlation leads to the prediction that **4** will undergo bowl-inversion more rapidly than

(1) Seiders, T. J.; Baldridge, K. K.; Grube, G. H.; Siegel, J. S. *J. Am. Chem. Soc.* **2001**, *123*, 517–525.

(2) The structure–energy correlation: (a) Bürgi, H. -B.; Dübler-Steuale, K. C. *J. Am. Chem. Soc.* **1988**, *110*, 4953–4957. (b) Bürgi, H. -B.; Dübler-Steuale, K. C. *J. Am. Chem. Soc.* **1988**, *110*, 7291–7299.

(3) Prefix *sym*- is used here to mean the C<sub>5</sub>-symmetric substituted corannulene corresponding to 1,3,5,7,9-pentasubstitution.

(4) Grube, G. H.; Elliott, E. L.; Steffens, R. J.; Jones, C. S.; Baldridge, K. K.; Siegel, J. S. *Org. Lett.* **2003**, *5*, 713.

(5) (a) Mislow, K.; Graeve, R.; Gordon, A. J.; Wahl, G. H., Jr. *Am. Chem. Soc.* **1964**, *86*, 1733. (b) Mislow, K.; Graeve, R.; Gordon, A. J.; Wahl, G. H., Jr. *J. Am. Chem. Soc.* **1963**, *85*, 1200. (c) Carter, R. E.; Melander, L. *Adv. Phys. Org. Chem.* **1973**, *10*, 1.

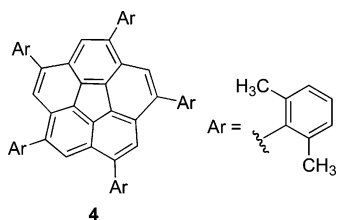
(6) For the crystallographic data, see Supporting Information (B).

1, consistent with the notions about a correlation between rim substitution and bowl depth or inversion barrier, but in sharp contrast to the experiment measurement.

Deeper analysis of the structure reveals how tricky the modeling of large organic systems can be. The hub, spoke, flank, and rim bond lengths display the normal [5]radialene pattern and are well reproduced by the B3LYP/cc-pVDZ level computations. The bond angles also display no serious anomalies. In general, the B3LYP/cc-pVDZ geometry of the corannulene core of **4** reflects crudely what one would expect from a structure with five aryl-ring substituents locked approximately orthogonal to the plane of the corannulene at the point of attachment.

Despite the good performance on basic geometric parameters, the barrier to bowl-inversion at the B3LYP/cc-pVDZ level is predicted to be 8.84 kcal/mol (ca 3 kcal/mol under the observed value). Thus in the absence of experiment, this level of theory would lead to erroneous conclusions about the bowl dynamics, that is, lower versus higher barrier than the parent corannulene.

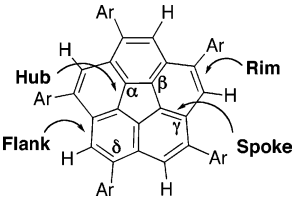
Although a single-point energy correction using the MP2 electron correlation treatment will not improve the geometry, it does provide the insight that inclusion of dispersion/dynamic correlation is very important to proper modeling of the inversion barrier. Augmentation of B3LYP/cc-pVDZ single-point energies with the DFT dispersion correction treatment of Grimme produced similar results.<sup>7</sup> From these results, one can infer that vdW stabilization of the bowl versus flat structure is at play.



**Structural Assessment of 3 and 4.** Ideally, one would like to reassess the geometry of these structures with the inclusion of such dispersion/dynamic correlation effects. At present, even with access to a very efficient parallel cluster computer, the memory and CPU requirements of such a job are formidable. Using the B3LYP/cc-pVDZ optimized structure for the input to an MP2 optimization looks promising as the gradient was only 0.0037 (a good guess en route to the  $10^{-6}$ – $10^{-7}$  criteria to claim “optimized”); however, each gradient cycle takes 11 days on a Dell PowerEdge 2950 quad core, consuming more than 30 GB memory and 1.6 TB disk, or 4 days on a dedicated dual core Itanium HP rx2600. The full optimizations complete in 47.5 days; however, Hessian analysis would be a second large investment in cpu time. In such a situation an implementation of a DFT code either with dispersion correction or functional parametrization should provide a more effective way to gain further insight at reasonable computational effort. The M06-2X functional is such a parametrized functional.<sup>8</sup>

Geometry optimization of **4** at M06-2X/cc-pVDZ was then carried out (Table 1). The agreement between B3LYP/cc-pVDZ and M06-2X/cc-pVDZ optimized structures leaves little to choose among bond lengths ( $<0.01$  Å difference) and bond angles ( $<1^\circ$  difference). The striking differences comes in the

**Table 1.** Computed Geometry of **4** Compared to Experimental Geometry of **3**



parameter	B3LYP/ cc-pVDZ <sup>a</sup>	M06-2X/ cc-pVDZ <sup>a</sup>	exptl
C–C hub (Å)	<b>1.418</b>	1.420	1.413(4)
C–C spoke (Å)	1.385	<b>1.381</b>	1.383(4)
C–C flank (Å)	1.461	<b>1.455</b>	1.452(4) leeward
	1.450	<b>1.446</b>	1.446(4) wayward
C–C rim (Å)	1.399	<b>1.388</b>	1.381(8)
angle $\alpha$ (sym) (deg)	108.0	108.0	108.0(4)
angle $\beta$ (deg)	<b>123.45</b>	122.85	124.3(4)
angle $\gamma$ (deg)	<b>114.77</b>	115.40	111.9(4)
angle $\delta$ (deg)	120.35	<b>120.56</b>	122.2(4)
bowl depth (Å)	0.854	<b>0.945</b>	0.91
Me <sub>(endo)</sub> (1)–Me <sub>(endo)</sub> (2) (Å)	4.62	<b>4.35</b>	4.4
Me <sub>(endo)</sub> (1)–Me <sub>(endo)</sub> (3) (Å)	7.60	<b>7.04</b>	7.1
Ar–Cor torsion (deg)	<b>79.6</b>	72.2	79

<sup>a</sup> Bold values in the theory columns indicate values closer to experimental results.

predicted bowl-depths (0.85<sub>4</sub> vs 0.94<sub>5</sub> Å), Me<sub>(endo)</sub>/Me<sub>(endo)</sub> nonbonded distances (4.62 vs 4.35 Å), and aryl-corannulene torsion angles (80.3° vs 72.0°).<sup>9</sup>

**X-ray Crystal Structure of 3.** Crystals of **3**, suitable for X-ray crystallographic analysis, were grown from a toluene/isopropanol solution by cooling. Diffraction data was collected at low temperature and the structure solved by direct methods. The solution revealed a resolvable whole molecule disorder in which two molecules of **3** are superposed on one another as enantiomeric models A and B (Figure 1). Although the idealized solution structure for **3** would be  $C_5$  symmetrical, unsymmetrical crystal packing distorts the bowl to an unsymmetrical shape consistent with its general position in the  $P1$  unit cell. The enantiomers are almost cylindrically symmetric from the perspective of their external steric presentation and as such pack into each other’s respective sites virtually interchangeably, leading to the observed occupational disorder in the crystal. This phenomenon is common for substituted corannulene structures. Nonetheless, the disorder model yields respectable R factors (0.045).

Despite the statistically respectable appearance of the crystal structure of **3**, one should look at the geometry of the individually derived enantiomeric model conformers with some degree of skepticism, and not use them as prima facie evidence for a structural feature that would be otherwise chemically unreasonable. In order to model the disordered structure, all chemically equivalent bond lengths and angles within and between both enantiomers were restrained to be similar during the refinement. As a result, the spread of values for parameters such as spoke, rim, hub, and flank bond lengths is very small. Beyond the issue of overlapping disorder, there is a substantial

(7) Grimme, S. *J. Chem. Phys.* **2006**, *124*, 034108.

(8) Zhao, Y.; Truhlar, D.G. *Theor. Chem. Acc.*, **2007**, *118*, DOI 10.1007/500214-007-0310-x.

(9) This comparison demonstrates the disservice done the community by studies founded only on bond lengths and angles and concluding that basis sets like 631-G\* serve to model structures as well as higher order methods. By focusing on the trivial aspects of structure, the uninitiated chemist could be led to unwarranted extrapolation of the model, which would inaccurately predict important structural parameters, dynamic character, and physical properties, see: Petrukhina, M. A.; Andreini, K. W.; Mack, J.; Scott, L.T. *J. Org. Chem.* **2005**, *70*, 5713.

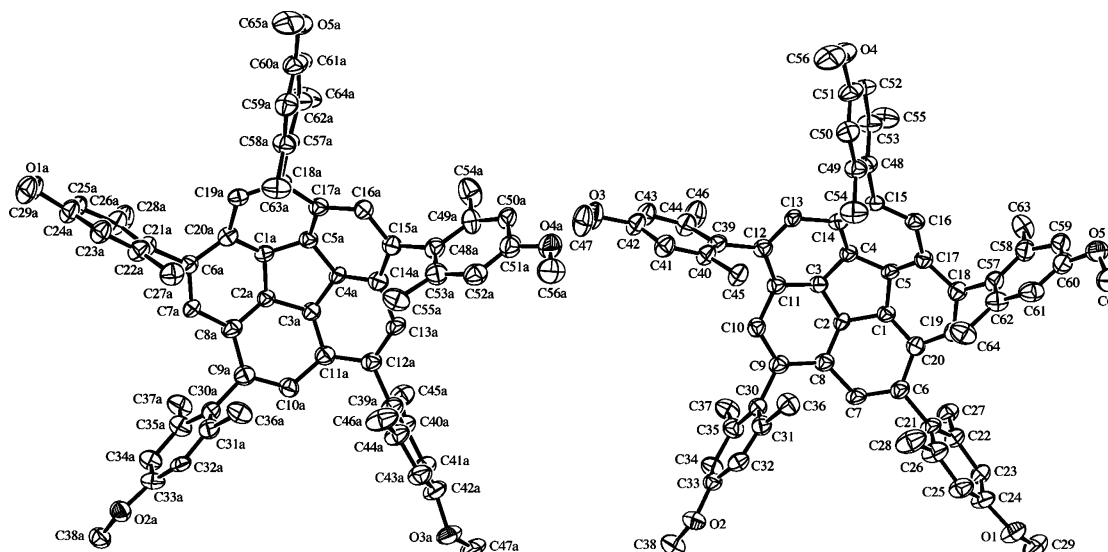


**Figure 1.** The molecular structure of **3** showing, separately, the two disordered enantiomeric species, which in the model are super-imposed on one another with the same center of gravity.

distortion away from 5-fold asymmetric geometry. This distortion has particular influence on the determination of a unique bowl depth. Although a singular bowl-depth<sub>hub-to-rim</sub> = 0.91 Å can be assigned by comparing the best plane of the hub to that of the rim, as is done for 5-fold symmetric structures, one finds that these two planes are not parallel in **3** and the individual rim-atom distances range from 0.86 to 1.05 Å. Given the expected highly sensitive  $\chi^4$  dependence of barrier to equilibrium bowl depth, it would be unwise to draw conclusions from such clearly contextually dependent data alone and/or without deeper analysis.

Bond lengths and angles are transferable parameters among cognate structures, but despite a relatively constant set of lengths and angles in **3** and **4** a wide spectrum of conclusions about the bowl depth and inversion dynamics are possible.<sup>10</sup> The restraints used during the refinement of the crystallographic model keep the ranges relatively small, but relevant comparisons can still be made of the average hub, spoke, flank, and rim bond lengths, and the  $\alpha$ ,  $\beta$ ,  $\gamma$ , and  $\delta$  angles (cf. Table 1). The experimental model presents chemically reasonable bond-length and angle parameters and appears to corroborate the general features predicted from theory at levels, which include electron correlation. For example, the geometry is consistent with the [5]radialene pattern normally observed in corannulenes. On average for **3**, the experimental bond lengths agree within 0.01 Å and angles within 1° of those predicted by either B3LYP/cc-pVDZ or M06-2X/cc-pVDZ for the analogue, **4**. Thus the relatively rigid features of the highly restrained crystallographic model look reliable.

The manisyl groups in **3** are situated more or less orthogonal to the bowl rim, but with a large spread of torsion angles: 65–89°. The average value, 79°, is more in line with the B3LYP/cc-pVDZ model, 80.3°, than the M06-2X/cc-pVDZ model, 72.0°, of **4**. The Me<sub>(endo)</sub>/Me<sub>(endo)</sub> distances in **3** range from 3.9 to 5.2 Å, reflecting a relatively large variance for the geometrical features dependent on soft potentials that can be altered by packing forces. Nonetheless, these values come to an average

of 4.4 Å, in line with the normal sum of methyl vdW radii, 4.4 Å, and more in line with the M06-2X/cc-pVDZ value of 4.35 Å than the B3LYP/cc-pVDZ value, 4.62 Å, for **4**.

Let us return to comment further on the bowl depth, which represents the minimum of a very soft potential but which cannot be averaged over several instances in the crystal. The comparison value for the bowl-depth in **3** is derived from the diffraction data (depth<sub>hub-to-rim</sub> = 0.912 Å) and sits between the M06-2X/cc-pVDZ value of 0.945 Å and the B3LYP/cc-pVDZ value of 0.854 Å. The magnitude of the difference alone is not the sole concern but rather the qualitative trend with regard to the parent corannulene; the X-ray and M06-2X/cc-pVDZ model suggest a deeper bowl for the pentaaryl derivative than corannulene, whereas the B3LYP/cc-pVDZ model suggests a shallower bowl. This difference goes to the heart of whether one would predict a higher or lower barrier compared to corannulene. Such a large geometric discrepancy among methods is not found for the parent corannulene (depth<sub>hub-to-rim</sub> = 0.873 Å [B3LYP/cc-pVDZ]; 0.887 Å [M06-2X/cc-pVDZ]; 0.887 Å [X-ray]). The deeper bowl depth and the closer positioning of Me<sub>(endo)</sub> groups in the crystal structure and M06-2X/cc-pVDZ model correlates with a cooperative stabilizing network of trans-bowl vdW interactions; an effect outside the scope of normal HF and density functional treatments.

**Computational Dynamics and Prediction of the Isotope Effect.** The ortho methyl groups of the aryl substituents in the bowl form of **3** or **4** belong to diastereotopic pentad sets, one with all members apart (exo) and one with all members convergent (endo) across the ring. This diastereotopic relationship provides the <sup>1</sup>H NMR probe necessary to measure the inversion barrier by DNMR methods.

Crystal structure analysis of **3** and M06-2X/cc-pVDZ computations of **4** place the neighboring endo methyl groups at essentially the vdW distance (ca. 4.5 Å), whereas the values across the ring contacts are about 7.0 Å. The structures of the exo set are much further separated at 6.5 and 10.5 Å, respectively. The proximity of the endo methyls in the bowl form is suspected to account for the unusual dynamic behavior due to stabilizing van der Waals interactions. In contrast to the

(10) For a discussion of flexible geometry in graphs with rigid distance relationships, see: Connelly, R. *Invent. Math.* **1982**, 66, 11.



**Table 2.** Inversion Energies of (**4**) from Computation

barrier	B3LYP/ cc-pVDZ	M06-2X/ cc-pVDZ	B3LYP/ cc-pVDZ+GD <sup>b</sup>	MP2/cc-pVDZ// B3LYP/cc-pVDZ <sup>c</sup>
no ZPE	9.05	13.15	13.83	14.09
CH <sub>3</sub> with ZPE <sup>a</sup>	8.84	12.65	13.62	13.88
CD <sub>3</sub> with ZPE <sup>a</sup>	8.88	12.72	13.66	13.92

<sup>a</sup> ZPE = zero point energy. <sup>b</sup> GD = dispersion ala Grimme;<sup>7</sup> taking the ZPE correction from the reference geometry. <sup>c</sup> Taking the ZPE correction from the reference geometry.

bowl, all the computed transition state models predict a flat form with the methyls separated from their nearest neighbors by at least 5–6 Å. At this distance vdW interactions should be greatly reduced. This analysis and the large difference among computed barriers to inversion (B3LYP/cc-pVDZ 8.84 kcal/mol vs [M06-2X/cc-pVDZ 12.65 kcal/mol; B3LYP/cc-pVDZ+Grimme dispersion = 13.62 kcal/mol; and MP2/cc-pVDZ//B3LYP/cc-pVDZ = 13.88 kcal/mol]) serve as the basis for the assumption that the vdW attractive forces play a role in fine-tuning the bowl-inversion barrier in **3**.

Computing the zero-point energy (ZPE) difference between **4-d**<sub>10</sub> (i.e., **4**-(CD<sub>Ar</sub>)<sub>10</sub>) and **4-d**<sub>30</sub> (i.e., **4**-(CD<sub>3</sub>)<sub>10</sub>) at M06-2X/cc-pVDZ leads to a prediction that the CD<sub>3</sub> compound will have a barrier to inversion ca. 0.074 kcal/mol higher than the parent (KIE = 1.16) (Table 2). Despite the clear prediction by computed ZPE differences and the existence of essential symmetry conditions needed to measure the barriers in **3-d**<sub>30</sub>, the paltry value of 70–80 cal/mol for  $\Delta\Delta H^\ddagger$  between **4-d**<sub>10</sub> and **4-d**<sub>30</sub> presents serious precision issues for a reliable experimental assessment of this prediction. An additional issue is the validity of using a simple ZPE argument for predicting the isotope effects in these systems. Thus came about the motivation to investigate more sophisticated theoretical methods for predicting the steric deuterium isotope effect.

**Experimental Design.** As mentioned above, the predicted small difference in energy creates a serious challenge to the design of an experiment that distinguishes a meaningful difference from random error. In the DNMR technique, the largest source of error comes from uncertainty in the measured temperature, not only in the precision of the temperature measure, but also the accuracy of the temperature measurement in the sample; placement of the sample relative to the thermocouple and rates of nitrogen gas flow can have a substantial influence. The amount of solvent and degree of equilibration time can also introduce problems when extremely accurate results are desired. Even when good calibration methods are used, there are still some errors that make it difficult to reduce the reproducibility error below 75 cal/mol for independent experiments, and if one considers three times the error as a significant difference, one would need error limits on the order of  $\pm 25$  cal/mol to test the prediction made above by H vs D ZPE analysis.

One solution for this problem would be to measure both molecules in the same tube at the same time, thus eliminating differences in temperature as a major source of error. To accomplish this, each of the compounds must have signals that decoalesce upon cooling of the sample, but do not overlap with any other signals in the mixture. Consideration of the equilibrium equation for the bowl inversion of **3** reveals that the methyl signals are not the only signals representing diastereotopic sets of protons; the signals for the aromatic protons neighboring the

methyl groups also belong to either endo or exo sets (Figure 2). Thus, a scheme of two complementary probe molecules can be derived from **3** by selective deuterium labeling in either the methyl hydrogen or aromatic hydrogen positions.

Deuteration of **3** at the aromatic positions maintains the same interaction between methyl groups as in the parent compound, allows the dynamic process to be followed through the coalescence of the diastereotopic methyl signals, and displays no peaks in the aromatic area of the <sup>1</sup>H NMR spectrum. In contrast, complete deuteration of **3** at the methyl positions establishes the necessary interaction among deuterated methyl groups, allows the dynamic process to be followed by coalescence of the diastereotopic aromatic protons, but has no peak in the methyl region of the <sup>1</sup>H NMR. Combination of **3**-(CD<sub>3</sub>)<sub>10</sub> with **3**-(D<sub>Ar</sub>)<sub>10</sub> presents the superposition of two “orthogonally” labeled spectra. As such, coalescence phenomena in the variable temperature DNMR experiment can be viewed for both compounds simultaneously without worry about the error due to temperature or the complication of signal overlap. To further minimize the error, the line shape can be followed over a large temperature interval and the final energy values reported for a temperature where the dynamic line shape is active for both compounds (i.e., in the middle of the temperature range).

**Synthesis.** Preparation of **3**-(CD<sub>3</sub>)<sub>10</sub> and **3**-(D<sub>Ar</sub>)<sub>10</sub> requires two basic tasks: (1) creation of the appropriately deuterated bromomanisyl and (2) effecting an efficient 5-fold aryl-corannulene coupling over *sym*-pentachlorocorannulene. Palladium coupling reactions are often used for the introduction of aryl (or alkyl) compounds because they normally proceed in relatively good chemical yield and display broad functional group tolerance. Such palladium chemistry dovetails well with the many kinds of halocorannulenes available from literature procedures (for example, 1,2,7,8-tetraiodocorannulene,<sup>11</sup> 1,2,7,8-tetrabromocorannulene,<sup>12</sup> bromocorannulene,<sup>13</sup> 2,3-dichlorocorannulene,<sup>14</sup> *sym*-pentachlorocorannulene (**5**),<sup>13</sup> and deca-chlorocorannulene<sup>13</sup>). Because of the low activity of chloride in these coupling reactions, the synthetic application of **5** requires some optimization. As no efficient synthesis of *sym*-pentabromocorannulene was obtained, optimization efforts were focused on the catalyst. Simple thermal activation was seen as the best option and therefore the thermally more stable *N*-heterocyclic carbene (NHC)-based catalyst of Nolan was chosen. This strategy proved effective, and our previously reported transformation of **5** into **3**, via nickel-catalyzed zinc-based Negishi coupling (7% yield),<sup>4</sup> could be improved to 18–35% by a modified Nolan protocol using the NHC ligand, 1,3-bis-(2,6-diisopropylphenyl)imidazoliumchloride (IPr·HCl) in combination with the zinc-based Negishi reagents (Scheme 1).<sup>15,16</sup>

The preparations of deuterated bromoanisoles are simple (Scheme 2). The synthesis of 1-bromo-4-methoxy-2,6-di(methyl-d<sub>3</sub>)benzene (**6**) started from dimethyl-5-methoxysophthalate (**7**)

- (11) Xu, G.; Sygula, A.; Marcinow, Z.; Rabideau, P. W. *Tetrahedron Lett.* **2000**, 41, 9931–9934.
- (12) Sygula, A.; Rabideau, P. W. *J. Am. Chem. Soc.* **2000**, 122, 6323–6324.
- (13) Seiders, T. J.; Baldrige, K. K.; Elliott, E. L.; Grube, G. H.; Siegel, J. S. *J. Am. Chem. Soc.* **1999**, 121, 7439–7440.
- (14) Seiders, T. J.; Elliott, E. L.; Grube, G. H.; Siegel, J. S. *J. Am. Chem. Soc.* **1999**, 121, 7804–7813.
- (15) Stille coupling: Grasa, G. A.; Nolan, S. P. *Org. Lett.* **2001**, 3, 119–122. Suzuki coupling: Navarro, O.; Kelly, R. A., III; Nolan, S. P.; *J. Am. Chem. Soc.* **2003**, 125, 16194–16195.
- (16) The synthesis of IPr·HCl: (a) Arduengo, A. J., III; Krafczyk, R.; Schmutzler, R.; *Tetrahedron* **1999**, 55, 14523–14534. (b) Jafarpour, L.; Stevens, E. D.; Nolan, S. P. *J. Organomet. Chem.* **2000**, 606, 49–54.

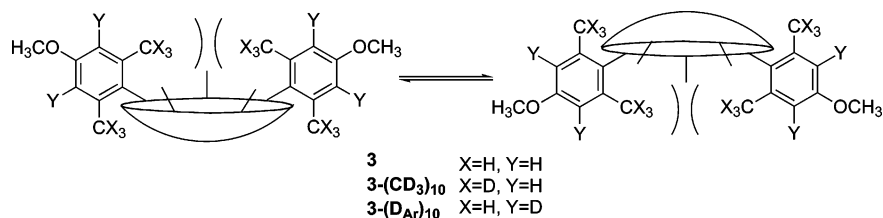
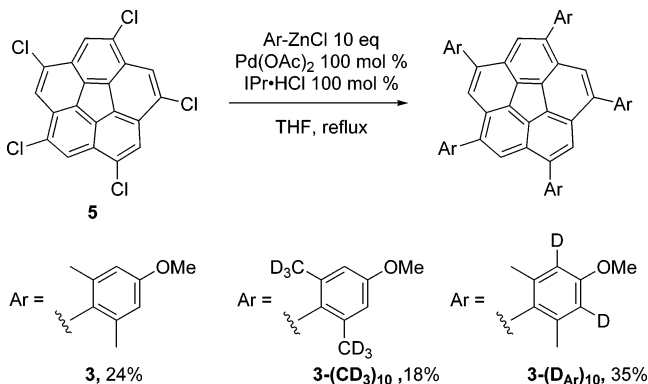


**Figure 2.** The equilibrium equation of **3**, **3-(CD<sub>3</sub>)<sub>10</sub>**, and **3-(DAr)<sub>10</sub>**.

**Scheme 1.** Synthesis of **3** and Deuterated Derivatives, **3-(CD<sub>3</sub>)<sub>10</sub>** and **3-(DAr)<sub>10</sub>**



by the reduction with lithium aluminum deuteride (LAD) (Scheme 2a). Then the diol **8** was mesylated with methanesulfonyl chloride and 4-(dimethylamino)pyridine (DMAP) and reduced with LAD again to form **9**. Finally the anisole was selectively brominated with *N*-bromosuccinimide (NBS) of the aromatic proton to afford **6**.<sup>17</sup>

The second deuterated bromoanisole 1-bromo-4-methoxy-2,6-dimethylbenzene-3,5-*d*<sub>2</sub> (**10**) was prepared with base-catalyzed hydrogen–deuterium exchange-reaction (Scheme 2b). First of all, the aromatic protons of 3,5-dimethylphenol (**11**) were deuterated using D<sub>2</sub>O and NaOD.<sup>18</sup> This process was repeated

five times until all aromatic protons were exchanged for deuteriums.<sup>19</sup> Then the deuterated phenol was methylated with iodomethane and potassium carbonate to give **12** followed by bromination with NBS to yield **9**.

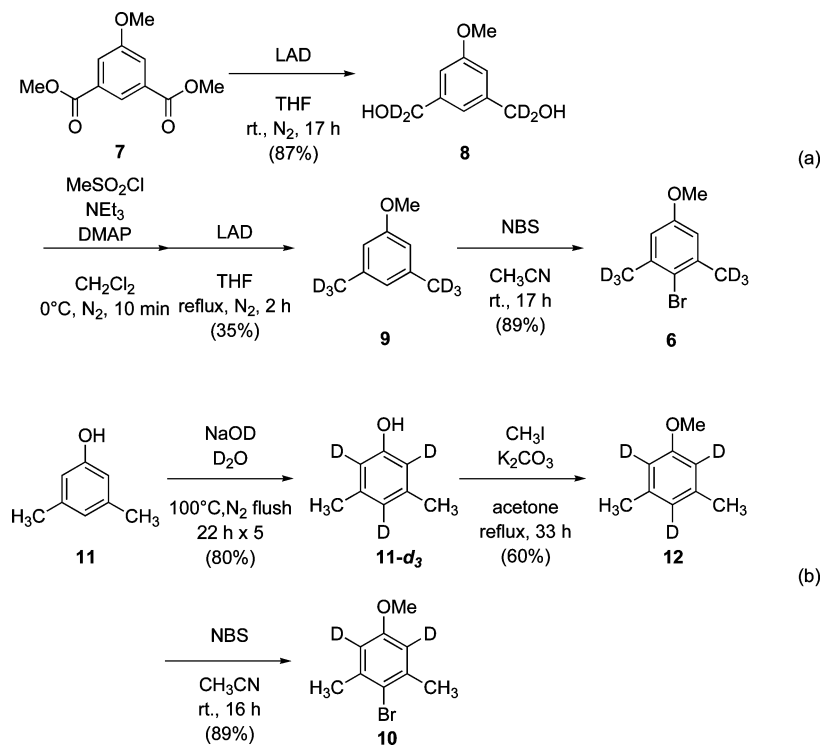
Having easy access to **6** and **10** meant the deuterated compounds **3-(CD<sub>3</sub>)<sub>10</sub>** and **3-(DAr)<sub>10</sub>** could be readily synthesized using the reaction conditions described above in Scheme 1. Mixing **3-(CD<sub>3</sub>)<sub>10</sub>** and **3-(DAr)<sub>10</sub>** created the necessary two-component probe for the DNMR experiment.

## Results and Discussion

**NMR Measurement of Isotope Effect.** From the mixture of **3-(CD<sub>3</sub>)<sub>10</sub>** and **3-(DAr)<sub>10</sub>** (**3-(CD<sub>3</sub>)<sub>10</sub>/3-(DAr)<sub>10</sub>** = 1/2.14) the variable temperature <sup>1</sup>H NMR spectra in dichloromethane-*d*<sub>2</sub> were obtained (Figure 3). For the evaluation of rate parameters, line-shape analysis of the aromatic protons of **3-(CD<sub>3</sub>)<sub>10</sub>** and the aromatic methyl protons of **3-(DAr)<sub>10</sub>** were used.<sup>20</sup> The inversion energies were compared at 250 K and at the respective coalescence temperatures.

The inversion energy of **3-(CD<sub>3</sub>)<sub>10</sub>** is found to be  $0.1 \pm 0.026$  kcal/mol larger than that of **3-(DAr)<sub>10</sub>** at 250 K, the midrange temperature where dynamic effects can be seen in the NMR (Table 3). This difference in inversion energy is greater than three times the sum of individual errors, placing it well above the 99% confidence limit as statistically significant. Under these statistical conditions, one would conclude that the experiment

**Scheme 2.**



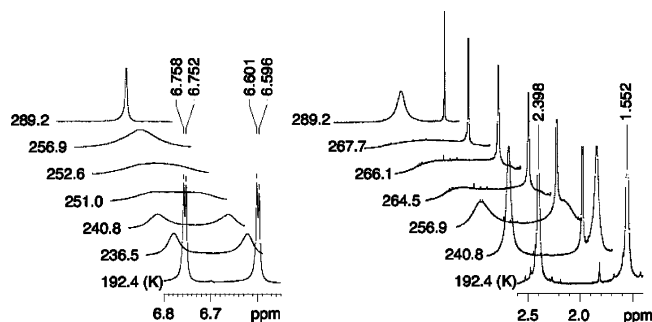


**Figure 3.** The aromatic proton peaks of **3**-(CD<sub>3</sub>)<sub>10</sub> (left) and the methyl proton peaks of **3**-(DAr)<sub>10</sub> (right) at different temperatures.

**Table 3.** The Inversion Energies of **3**-(CD<sub>3</sub>)<sub>10</sub> and **3**-(DAr)<sub>10</sub> from Line-Shape Analysis in Dichloromethane-*d*<sub>2</sub>

	<i>T</i> <sub>c</sub> (K)	Δ <i>G</i> <sub>T250</sub> <sup>‡</sup> (kcal/mol)	Δ <i>G</i> <sub>Tc</sub> <sup>‡</sup> (kcal/mol)
<b>3</b> -(DAr) <sub>10</sub> (CH <sub>3</sub> ) <sup>a</sup>	266.1	11.62 ± 0.015	11.60 ± 0.011
<b>3</b> -(CD <sub>3</sub> ) <sub>10</sub> (CD <sub>3</sub> ) <sup>b</sup>	251.0	11.72 ± 0.011	11.72 ± 0.010

<sup>a</sup> Calculated from methyl proton peaks. <sup>b</sup> Calculated from aromatic proton peaks.

demonstrates a clear direction and magnitude of the isotope effect (cf. Table 1), thus dealing with one of the main issues of this study. It also happens that the value found experimentally matches qualitatively that predicted by simple ZPE analysis; however, a proper analysis of the theoretical isotope effect is instructive.

**Computation of Isotope Effect.** Proper values for the kinetic isotope effect (KIE) were calculated using a modified version of the QUIVER software package, utilizing the optimized ground and transition-state structure vibrational analyses of **4**. On the basis of statistical mechanics and classical transition state theory, reduced partition functions of the various isotopomers are calculated from the force constants using the Biegeleisen–Mayer formalism:<sup>21</sup>

$$\frac{k_{\text{H}}}{k_{\text{D}}} = \frac{\kappa_{\text{H}} \sigma_{\text{H}} \sigma_{\text{H}}^*}{\kappa_{\text{D}} \sigma_{\text{D}} \sigma_{\text{D}}^*} (\text{mmi})(\text{exc})(\text{zpe})$$

where mmi is the mass and moment of inertia, exc is the excitation factor, zpe is the zero-point energy, and  $\sigma^*$  refers to the transition state. Using standard assumptions (mmi = 1;  $\kappa$  and  $\sigma$  unchanged in the various isotopomers), one then applies the Redlich–Teller product rule and substitutes explicit terms for the partition functions, using the ratios of the Biegeleisen–Mayer functions,  $(s_2/s_1)f(2/1)$  for the various isotopomers. The predicted KIE, without any tunneling correction, is simply

$$\frac{k_{\text{H}}}{k_{\text{D}}} = \frac{\nu_{\text{H}}^* (s_2/s_1) f(2/1)}{\nu_{\text{D}}^* (s_2/s_1) f(2/1)^*}$$

for all ratios and frequency values. To include effects of tunneling, thermally averaged transmission coefficients for an infinite parabolic barrier are calculated as approximated by Bell

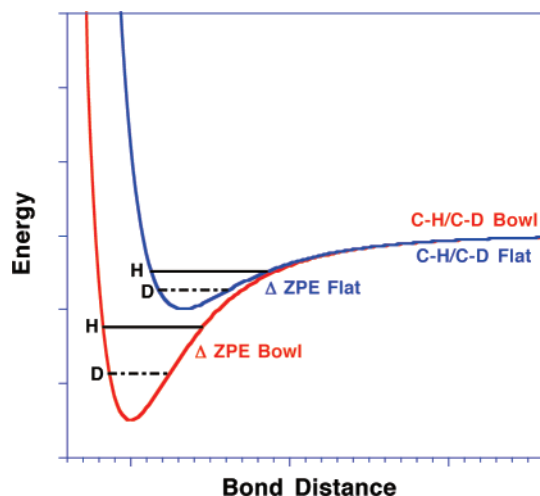


**Figure 4.** Differential ZPE for C–D and C–H in the bowl and flat forms.

(KIE/ip).<sup>22</sup> This treatment provides KIE for individual sites of deuterium substitution. Treating these single-site KIEs as energetically additive requires one to take the product over the 30 methyl C–H sites together to obtain a value for **4**-(CD<sub>3</sub>)<sub>10</sub>; similarly, one must take the product over the 10 aryl C–H sites to obtain a value for **4**-(DAr)<sub>10</sub>. Such an analysis gives 1.071 for the KIE/ip of **4**-(CD<sub>3</sub>)<sub>10</sub> and 0.996 for **4**-(DAr)<sub>10</sub>. The ratio of these KIE/ip values is suitable for comparison with experiment.

The comparison can be conducted either by converting the ΔΔ*G*<sup>‡</sup> of experiment into a KIE ratio or converting the theoretical KIE ratio into a ΔΔ*G*<sup>‡</sup>. The former leads to an experimental KIE of 1.22 ± 0.06 which compares qualitatively with the 1.08 obtained from the ratio just described. The equivalent analysis based on ΔΔ*G*<sup>‡</sup> yields a theoretical value of 0.04 kcal/mol in comparison with the 0.10 ± 0.026 kcal/mol reported from the variable temperature NMR experiments above.

These values are determined for 250 K to match the midrange temperature at which the experimental determination was made. With many low-energy vibration/libration modes as in **4**, it is likely that entropic effects will alter the KIE with temperature.

**Model for Interpreting the Isotope Effect.** Independent of the statistical success of these results, one would like a physical model to understand steric isotope effects. The prevailing model from quantum mechanics is that, although hydrogen and deuterium give rise to the same potential-energy surface, the ZPE for the motions of deuterium sits lower in the well than hydrogen. The result is that in a competition between two states with wells of different steepness, the deuterium ZPE favors the steeper well energetically (Figure 4). In principle, all H/D isotope effects can be interpreted in this way as a first approximation. Other considerations such as tunneling come into the full treatment, as described above.

The ZPE interpretation of steric isotope effects has precedence in the recent literature regarding cyclohexane inversions<sup>23</sup> and host–guest chemistry.<sup>24</sup> Historically, there have been notions of the CD<sub>3</sub> group being smaller than CH<sub>3</sub>. From the asymmetric bonding potential-energy well of the C–H bond, the lower C–D

(17) Edwards, J. D., Jr.; Cashaw, J. L. *J. Am. Chem. Soc.* **1956**, *78*, 3821–3824.

(18) Wähälä, K.; Mäkelä, T.; Bäckström, R.; Brunow, G.; Hase, T. *J. Chem. Soc., Perkin Trans. 1* **1986**, *1*, 95–98.

(19) From H-NMR, 99% deuterium displacements were confirmed.

(20) For the detail of the line shape analysis, see Supporting Information (A).

(21) Biegeleisen, J.; Mayer, M. G. *J. Chem. Phys.* **1947**, *51*, 1369–1374.

(22) Bell, R.P. *The Tunnel Effect in Chemistry*; Chapman and Hall: New York, 1980, pp 60–63.

(23) Saunders, M.; Wolfsberg, M.; Anet, F. A. L.; Kronja, O. *J. Am. Chem. Soc.* **2007**, *129*, 10276.



stretch yields a shorter  $r_{\text{eq}}$  for C–D than for C–H. Therefore, the vdW radii for  $\text{CD}_3$  is presumed to be smaller than for  $\text{CH}_3$ .<sup>5,25,26</sup> This notion focuses only on the effect of the stretching modes; however, the isotope effect comes from the sum over all modes involving H/D motion, including wags, librations, and rotations and is sensitive to the steepness of the potential in all dimensions.

The issue of changing the steepness of the potential-energy surface is important in molecular recognition. First, consider the case in which the neighboring  $\text{CH}_3/\text{CH}_3$  distance would be shorter than the sum of the vdW radii. Then the resting position of the corannulene bowl would be holding the methyls of the manisyl groups inside the sum of vdW radii to overcome a repulsion between methyl groups and arrive at a higher energy (strained) equilibrium geometry. Therefore, shorter distances between methyl groups would lead to a compression that should increase the steepness of the C–H potential. If the changes in that mode dominate, then the bowl with  $\text{CD}_3$  would be lower in energy compared to the flat transition state, where such interactions are much less important. The barrier for **3**-( $\text{CD}_3$ )<sub>10</sub> should be higher than the barrier for **3**-( $\text{D}_{\text{Ar}}$ )<sub>10</sub>.

Second, consider the case in which the neighboring  $\text{CH}_3/\text{CH}_3$  distance would be longer than the sum of vdW radii for  $\text{CH}_3$ . In this case, the resting position of the corannulene bowl would favor placement of the methyl groups outside the sum of vdW radii and an attraction between the methyls helps establish the equilibrium geometry. Key here is not the attractive or repulsive component between the methyls, but rather the affect their proximity has on the steepness of the potential. Indeed, long before the methyl groups come to the point of vdW contact, their vibrations interact, leading to a steepening of the well and an energetic bias for deuterium in the bowl form. This model is supported by the detailed analysis of the KIE prediction, which says that on the endo methyl groups, the CH bond vector pointing into the bowl favors a KIE > 1, whereas the one pointing away from the bowl favors KIE ≤ 1.

The simple ZPE difference analysis is consistent with the barrier for **3**-( $\text{CD}_3$ )<sub>10</sub> being higher than the barrier for **3**-( $\text{D}_{\text{Ar}}$ )<sub>10</sub>. Nonetheless, the phenomenology suggests that the vdW attraction of  $\text{CD}_3/\text{CD}_3$  is larger, which could lead to the notion of  $\text{CD}_3$  being “stickier” (i.e., more tightly bound). A parallel to this concept can be found in the higher binding constants measured for deuterated host–guest systems.<sup>24</sup>

As both of these scenarios can be rationalized by a ZPE effect in the same direction, the isotope effect as sole factor cannot indicate whether the trans-bowl methyl interaction is attractive or repulsive. Both situations can be approximated by a vibrating C–H oscillator such that when two or more such oscillators come into proximity, their space becomes restricted and the potential-energy well becomes steeper. The larger energy spacings for the steeper well makes a ZPE bias for C–D over C–H. The shape of quantum mechanical potential-energy surface is identical for C–H and C–D. In short, the bowl form of **3** presents a more congested methyl environment than the

flat transition state; deuterium favors the bowl form and manifests a higher barrier.

The conclusion that the methyl interactions contribute in an attractive way comes from the observation that the  $\text{C}_{20}$  bowl in **3** and **4** is deeper than in **1**, and the barrier to inversion of **3** and **4** is higher than **1**. “Normal” repulsive steric effects at the rim of **1** would work in the opposite direction structurally and energetically. Thus the trans-bowl interactions provide insight to the nature of noncovalent interactions and a gauge of their energetic magnitude.

## Conclusions

An anomalous barrier height in the bowl-inversion of **3** leads to the hypothesis that attractive vdW interactions are at play in the dynamics of **3**. Computational results supporting this hypothesis stimulated the idea that study of the dynamics in isotopomers of **3** could result in an estimate of an attractive deuterium steric isotope effect. To this end, an isotope-based symmetry analysis leads to the design of an experiment in which the dynamics of two orthogonally labeled isotopomers of **3** could be measured simultaneously to enable a variable temperature NMR determination of  $\Delta\Delta G^\ddagger$  values with high accuracy. These energies correlate with KIE ratios. Analysis of the KIE using quantum mechanical optimized structures for the ground and transition states in combination with a computational KIE prediction (modified QUIVER) leads to values in reasonable agreement with those obtained experimentally. The isotope effect is seen to come from a differential ZPE between flat and bowl forms owing to the general increase in the steepness of the interaction potential between methyl groups in a crowded environment.

In the course of this work, it was necessary to develop a synthetic methodology for pentasubstitution of *sym*-pentachlorocorannulene. This was achieved in relatively good chemical yield using Negishi reagents and palladium with Nolan’s NHC ligands. This result shows the usefulness of the NHC ligand even for the coupling reaction with multichlorides.

Transannulene interactions in bowl-shaped compounds should provide a general arena for studying molecular recognition. Other *sym*-substituted corannulenes may be anticipated as model compounds for the investigation other interactions.

## Methods

**Computational Methods.** The conformational analyses of the molecular systems described in this study, including structural and orbital arrangements as well as property calculations, were carried out using the Gaussian 98<sup>27</sup> and GAMESS<sup>28</sup> software packages. Structural computations of all compounds were performed using hybrid density functional methods (HDFT). The HDFT method employed Becke’s 3 parameter functional<sup>29</sup> in combination with nonlocal correlation provided by the Lee–Yang–Parr expression<sup>30,31</sup> with both local and nonlocal terms, B3LYP, as well as the new M06-2X functional of Truhlar et al.<sup>8</sup> Dunning’s correlation consistent basis set, cc-pVDZ, a [3s2p1d] contraction of a (9s4p1d) primitive set was employed.<sup>32</sup> Full

- (24) (a) Zhao, Y.-L.; Houk, K. N.; Rechavi, D.; Scarso, A.; Rebek, J., Jr. *J. Am. Chem. Soc.* **2004**, *126*, 11426. (b) Laughrey, Z. R.; Upton, T. G.; Gibb, B. C. *J. Chem. Soc., Chem. Commun.* **2006**, 970. (c) Liu, Y.; Warmuth, R. *Org. Lett.* **2007**, *9*, 2883.  
(25) Ubbelohde, A. R. *Trans. Faraday Soc.* **1936**, *32*, 525.  
(26) Pauling, L. *The Nature of the Chemical Bond*; Graphic Reproductions Ltd: London, 1952; Chapter 5.

- (27) Frisch, M. J.; et al. *Gaussian 98*, Revision A.6, Gaussian, Inc.: Wallingford, CA, 1998.  
(28) Schmidt, M. W.; Baldridge, K. K.; Boatz, J. A.; Elbert, S. T.; Gordon, M. S.; Jensen, J. H.; Koseki, S.; Matsunaga, N.; Nguyen, K. A.; Su, S.; Windus, T. L.; Elbert, S. T. *J. Comp. Chem.* **1993**, *14*, 1347.  
(29) Becke, A. D. *J. Chem. Phys.* **1993**, *98*, 5648–5652.  
(30) Lee, C.; Yang, W.; Parr, R. G. *Phys. Rev. B* **1988**, *37*, 785.  
(31) Miehlich, B.; Savin, A.; Stoll, H.; Preuss, H. *Chem. Phys. Lett* **1989**, *157*, 200.  
(32) Dunning, T. H. *J. Chem. Phys.* **1989**, *90*, 1007.

geometry optimizations were performed with an ultrafine grid and tight criteria and uniquely characterized via second derivatives (Hessian) analysis to determine the number of imaginary frequencies (0 = minima; 1 = transition state), zero point contributions. Additionally, deuterium isotopic difference effects were determined from selective deuterium substitutions made on the aryl and methyl groups as described in the text. From the fully optimized structures, single point energy and gradient computations were performed using the MP2 dynamic correlation treatment,<sup>33</sup> providing more accurate energy barriers and insight into the difference from optimization, respectively. We have established these levels of theory to be reliable for structural and energetic determinations in these types of compounds in several previous publications.<sup>34</sup> Analysis using the Grimme DFT dispersion method was accomplished by implementation of the recently developed methodology of Grimme into our GAMESS software. More sophisticated kinetic analysis was done using a modified version of QUIVER (frequency scaling factor 0.9614 and temperature = 250 K),<sup>35</sup> which provides calculation of the kinetic isotope effect corrected for tunneling with a one-dimensional tunneling approximation, as proposed by Bell.<sup>22</sup> Corrections were introduced in accord with a recent book chapter by M. Wolfsberg.<sup>36</sup> Molecular orbital and electrostatic contour plots, used as an aid in the analysis of results, were generated and depicted using the programs 3D-PLTORB<sup>37</sup> and QMView.<sup>38</sup>

**Experimental Methods. General.** Data were collected on the following instruments: <sup>1</sup>H and <sup>13</sup>C NMR, Bruker AMX 300 (300 and 75.5 MHz); IR, Bruker IFS 66 (FT-IR); EI-MS, Finnegan MAT 95 spectrometer (70 eV). High-resolution mass data (HRMS) were obtained by preselected-ion peak matching at  $R \approx 10000$  to be within  $\pm 3$  ppm of the exact mass. Crystallographic data was recorded using a Nonius Kappa CCD diffractometer with Mo K $\alpha$  radiation ( $\lambda = 0.71073$  Å). Chromatography was performed using Merck silica gel 60 (230–400 mesh) or Fluka neutral alumina (Brockmann I, Activity II). Tetrahydrofuran (THF) was distilled from sodium/benzophenone. Solvents for chromatography were technical grade and freshly distilled before use. *sym*-Pentachlorocorannulene<sup>4</sup> and IPr·HCl<sup>16</sup> were prepared according to the literature procedures. Other compounds, which are not mentioned in the experimental section and Supporting Information, are commercially available.

**5-Methoxybenzenebis(methane- $\alpha,\alpha$ -d<sub>2</sub>)-ol (8).** To a suspension of LAD (4.62 g; 110 mmol) in THF (100 mL), dimethyl-5-methoxyisophthalate (11.2 g, 50 mmol) in THF (150 mL) was added dropwise. The mixture was stirred at room temperature (rt) for 17 h under nitrogen. After cooling to 0 °C, an aqueous solution of H<sub>2</sub>SO<sub>4</sub> (175 mL, 1 M) was added. The mixture was diluted with ethylacetate (100 mL), separated, washed with saturated aqueous NaCl (100 mL), dried with Na<sub>2</sub>SO<sub>4</sub>, and evaporated to yield a white solid (7.50 g; 87%) of **8**: mp 79 °C. IR (KBr)  $\nu$  cm<sup>-1</sup>: 3330, 3203, 1596, 1460, 1429, 1339, 1296, 1200, 1173, 1102, 1056, 966, 856, 816, 800, 690. <sup>1</sup>H NMR (300 MHz, CDCl<sub>3</sub>):  $\delta$  ppm: 1.62 (s, 2H), 3.83 (s, 3H), 6.86 (d, <sup>3</sup>J = 1.5 Hz, 2H), 6.96 (t, <sup>3</sup>J = 1.5 Hz, 1H). <sup>13</sup>C NMR (75.5 MHz, CDCl<sub>3</sub>, plus DEPT):  $\delta$  ppm: 55.2 (CH<sub>3</sub>), 64.1 (quint, <sup>1</sup>J = 22.2 Hz, CD<sub>2</sub>), 111.5 (CH), 117.5 (CH), 142.6 (C), 159.8 (C). MS (EI),  $m/z$  (%): 172 (M<sup>+</sup>), 139 (M<sup>+</sup> – CD<sub>2</sub>OH). HRMS (EI): calcd for C<sub>9</sub>H<sub>8</sub>D<sub>4</sub>O<sub>3</sub>, 172.1038; found, 172.1038.

**1-Methoxy-3,5-di(d<sub>3</sub>-methyl)benzene (9).** To a solution of **8** (5.17 g, 30 mmol), DMAP (750 mg, 6 mmol), and triethylamine (12.6 mL, 90 mmol) in dichloromethane (300 mL), methanesulfonyl chloride (6.9

mL, 90 mmol) was added dropwise with stirring at 0 °C under nitrogen. The mixture was stirred at 0 °C for 10 min under nitrogen. The reaction was quenched with the addition of water (150 mL). The organic layer was separated, dried with Na<sub>2</sub>SO<sub>4</sub>, and evaporated to yield a pale yellow oil (10.1 g). To a suspension of LAD (5.67 g, 135 mmol) in THF (80 mL), the crude mixture in THF (120 mL) was added dropwise over a period of 30 min at rt under nitrogen. The mixture was heated at 60 °C for 2 h under nitrogen. After the mixture was cooled to 0 °C, an aqueous solution of H<sub>2</sub>SO<sub>4</sub> (300 mL, 1 M) was added. The mixture was diluted with ethylacetate (50 mL), filtered, separated, washed with saturated aqueous NaCl (100 mL), dried with Na<sub>2</sub>SO<sub>4</sub>, and evaporated to yield a yellow oil (2.95 g). The product was purified by column chromatography on silica gel eluted with hexane. The solvent was evaporated to yield a colorless oil (1.50 g; 35%) of **9** [ $R_f$  = 0.85 (SiO<sub>2</sub>, hexane/ethyl acetate = 16:1)]. IR (KBr):  $\nu$  cm<sup>-1</sup> = 1610, 1592, 1453, 1433, 1327, 1299, 1196, 1164, 1073, 1046, 908, 785, 678, 580. <sup>1</sup>H NMR (300 MHz, CDCl<sub>3</sub>):  $\delta$  ppm = 3.77 (s, 3H), 6.53 (d, <sup>3</sup>J = 1.5 Hz, 2H), 6.60 (t, <sup>3</sup>J = 1.5 Hz, 1H). <sup>13</sup>C NMR (75.5 MHz, CDCl<sub>3</sub>, plus DEPT):  $\delta$  ppm = 20.5 (septet, <sup>1</sup>J = 19.1 Hz, CD<sub>3</sub>), 55.0 (CH<sub>3</sub>), 111.7 (CH), 122.4 (CH), 139.0 (C), 160.0 (C). MS (EI),  $m/z$  (%): 142 (M<sup>+</sup>), 124 (M<sup>+</sup> – CD<sub>3</sub>), 111 (M<sup>+</sup> – OCH<sub>3</sub>).

**1-Bromo-4-methoxy-2,6-di(d<sub>3</sub>-methyl)benzene (6).** A solution of NBS (1.69 g, 9.5 mmol) in acetonitrile (15 mL) was added dropwise to **9** (1.42 g, 10 mmol) in acetonitrile (5 mL) at 0 °C. After warming to rt and stirring for 17 h, water (20 mL) was added. The mixture was extracted with hexane (50 mL  $\times$  4), dried with Na<sub>2</sub>SO<sub>4</sub>, and evaporated to yield a yellow oil (1.96 g; 89%) of **6**. IR (KBr)  $\nu$  cm<sup>-1</sup>: 1584, 1448, 1427, 1413, 1326, 1584, 1448, 1427, 1413, 1326, 1198, 1168, 1049, 1014, 826. <sup>1</sup>H NMR (300 MHz, CDCl<sub>3</sub>)  $\delta$  ppm: 3.76 (s, 3H), 6.64 (s, 2H). <sup>13</sup>C NMR (75.5 MHz, CDCl<sub>3</sub>, plus DEPT)  $\delta$  ppm: 23.1 (septet, <sup>1</sup>J = 19.5 Hz, CD<sub>3</sub>), 55.2 (CH<sub>3</sub>), 113.8 (C), 122.4 (CH), 138.9 (C), 158.0 (C). MS (EI),  $m/z$  (%): 221 (M<sup>+</sup>), 141 (M<sup>+</sup> – Br), 111 (M<sup>+</sup> – OCH<sub>3</sub> – Br). HRMS (EI): calcd for C<sub>9</sub>H<sub>5</sub>D<sub>6</sub>BrO. 220.0370; found, 220.0367.

**3,5-Dimethylphen-2,4,6-d<sub>3</sub>-ol (11-d<sub>3</sub>).** 3,5-Dimethylphenol (6.11 g, 50 mmol), deuterium oxide (8.94 mL, 500 mmol), and sodium deuterioxide (1 mL, 40 wt % solution in D<sub>2</sub>O) were placed in a pressure tube (Ace pressure tube from Aldrich). After the nitrogen flush, the tube was sealed and heated at 100 °C for 22 h. After cooling to 0 °C, the reaction mixture was acidified with concentrated H<sub>2</sub>SO<sub>4</sub> (3 mL) in D<sub>2</sub>O (7 mL). The resulting precipitate was filtered and washed with D<sub>2</sub>O (2 mL  $\times$  5). This process was repeated an additional four times to yield a brown solid (5.01 g; 79%) of **11-d<sub>3</sub>**: mp 51–52 °C. IR (KBr)  $\nu$  cm<sup>-1</sup>: 3275, 2434, 1597, 1575, 1448, 1390, 1311, 1053, 547. <sup>1</sup>H NMR (75.5 MHz, CDCl<sub>3</sub>, plus DEPT)  $\delta$  ppm: 2.60 (s, 6H). <sup>13</sup>C NMR (75.5 MHz, CDCl<sub>3</sub>, plus DEPT)  $\delta$  ppm: 21.0 (CH<sub>3</sub>), 112.7 (t, <sup>1</sup>J = 21.8 Hz, CD), 122.1 (t, <sup>1</sup>J = 23.3 Hz, CD), 139.3 (C), 155.2 (C). MS (EI),  $m/z$  (%): 126 (M<sup>+</sup>), 111 (M<sup>+</sup> – CH<sub>3</sub>). HRMS (EI): calcd for C<sub>8</sub>H<sub>6</sub>D<sub>4</sub>O, 126.0983; found, 126.0980.

**1-Methoxy-3,5-dimethylbenzene-2,4,6-d<sub>3</sub> (12).** To a suspension of **11-d<sub>3</sub>** (5.01 g, 40 mmol) in acetone (90 mL), potassium carbonate (22.2 g, 160 mmol) and iodomethane (12.5 mL, 200 mmol) were added. The mixture was heated at 75 °C for 33 h. After cooling to rt, the solvent was evaporated. Water (70 mL) was added, and the mixture was extracted with ethylacetate (100 mL). The organic layer was washed with water (70 mL) and saturated aqueous NaCl (70 mL), dried with MgSO<sub>4</sub>, and evaporated to yield **12** as a brown oil (3.36 g; 60%). IR (KBr)  $\nu$  cm<sup>-1</sup>: 2955, 2926, 2874, 2861, 826, 724. <sup>1</sup>H NMR (300 MHz, CDCl<sub>3</sub>)  $\delta$  ppm: 2.84 (s, 6H), 3.71 (s, 3H). <sup>13</sup>C NMR (75.5 MHz, CDCl<sub>3</sub>, plus DEPT)  $\delta$  ppm: 21.3 (CH<sub>3</sub>), 55.0 (CH<sub>3</sub>), 111.5 (t, <sup>1</sup>J = 23.9 Hz, CD), 122.2 (t, <sup>1</sup>J = 23.9 Hz, CD), 139.0 (C), 159.6 (C). MS (EI),  $m/z$  (%): 139 (M<sup>+</sup>), 124 (M<sup>+</sup> – CH<sub>3</sub>), 108 (M<sup>+</sup> – OCH<sub>3</sub>).

**1-Bromo-4-methoxy-2,6-dimethylbenzene-3,5-d<sub>2</sub> (10).** A solution of NBS (3.63 g, 20.4 mmol) in acetonitrile (30 mL) was added dropwise to **12** (2.92 g, 21 mmol) in acetonitrile (10 mL) at 0 °C. After warming to rt and stirring for 16 h, water (30 mL) was added. The mixture was

(33) Moller, C.; Plesset, M. S. *Phys. Rev.* **1934**, *46*, 618–622.

(34) For example, see Seiders, T. J.; Baldrige, K. K.; Grube, G. H.; Siegel, J. S. *J. Am. Chem. Soc.* **2001**, *123*, 517–525.

(35) Saunders, M.; Laidig, K. E.; Wolfsberg, M. *J. Am. Chem. Soc.* **1989**, *111*, 8989–8994.

(36) Wolfsberg, M. Comments on Selected Topics in Isotope Theoretical Chemistry. In *Isotope Effects in Chemistry and Biology*; Amnon Kohen, A., Hans-Heinrich Limbach, H.-H., Eds.; CRC Press/Taylor & Francis: Boca Raton, FL, 2005; Chapter 3.

(37) *3D-PLTORB, version 3D*; San Diego Supercomputer Center: San Diego, CA, 1997.

(38) Baldrige, K. K.; Greenberg, J. P. *J. Mol. Graphics* **1995**, *13*, 63.



extracted with hexane (20 mL  $\times$  5), dried with  $\text{MgSO}_4$ , and evaporated to yield an orange oil (4.03 g; 24%) of **10**. IR (KBr)  $\nu$   $\text{cm}^{-1}$ : 1566, 1456, 1437, 1378, 1320, 1110, 1013.  $^1\text{H}$  NMR (300 MHz,  $\text{CDCl}_3$ )  $\delta$  ppm: 2.38 (s, 6H), 3.76 (s, 3H).  $^{13}\text{C}$  NMR (75.5 MHz,  $\text{CDCl}_3$ , plus DEPT)  $\delta$  ppm: 23.9 ( $\text{CH}_3$ ), 55.2 ( $\text{CH}_3$ ), 113.5 (t,  $^1J = 24.2$  Hz, CD), 118.1 (CH), 138.9 (C), 158.0 (C). MS (EI),  $m/z$  (%): 217 ( $\text{M}^+$ ), 202 ( $\text{M}^+ - \text{Br} - \text{CH}_3$ ), 137 ( $\text{M}^+ - \text{Br}$ ), 107 ( $\text{M}^+ - \text{Br} - \text{OCH}_3$ ). HRMS (EI): calcd for  $\text{C}_9\text{H}_9\text{D}_2\text{BrO}$ , 216.0119; found, 216.0115.

**sym-Pentamanisylcorannulene (3).** 4-Bromo-3,5-dimethylanisole (153 mg, 0.71 mmol) in THF (10 mL) was cooled to  $-78^\circ\text{C}$  in a dry ice/acetone bath and *n*-butyllithium (0.52 mL, 0.78 mmol) was added as a 1.5 M solution in hexane. After 30 min, a freshly prepared solution of  $\text{ZnCl}_2$  (146 mg, 1.07 mmol) in THF (5 mL) was transferred to the solution. The mixture was stirred in the dry ice/acetone bath for 10 min and the bath was removed. After an additional 20 min, the resulting aryl-zinc chloride solution was transferred to a flask containing a suspension of *sym*-pentachlorocorannulene (30 mg, 0.071 mmol),  $\text{Pd}(\text{OAc})_2$  (16 mg, 0.071 mmol), and  $\text{IPr}\cdot\text{HCl}$  (30 mg, 0.071 mmol) in THF (5 mL). The mixture was refluxed at  $110^\circ\text{C}$  in an oil bath for 4 days. The cooled mixture was filtered over celite and washed with dichloromethane. The mixture was evaporated. The product was purified by column chromatography on aluminum oxide (5% deactivated with water) eluted with hexane/dichloromethane at 3/1, 2/1, and 1.5/1. The solvent was evaporated to yield **3** as a yellow solid (0.16 g; 89%) **3** [ $R_f = 0.35$  ( $\text{Al}_2\text{O}_3$ , hexane/dichloromethane = 3:1)]. The spectroscopic data were identical with those reported.<sup>4</sup>

**sym-Penta(4-methoxy-2,6-di(methyl- $d_3$ )phenyl)corannulene (3-( $\text{CD}_3$ )<sub>10</sub>).** The similar procedure to the synthesis of **3** yielded a yellow solid (18%) of **3-(CD<sub>3</sub>)<sub>10</sub>**: mp  $>350^\circ\text{C}$ . IR (KBr)  $\nu$   $\text{cm}^{-1}$ : 3444, 1600, 1465, 1420, 1320, 1196, 1170, 1046.  $^1\text{H}$  NMR (75.5 MHz,  $\text{CDCl}_3$ , plus DEPT)  $\delta$  ppm: 3.81 (s, 15H), 6.66 (s, 10H), 7.10 (s, 5H).  $^{13}\text{C}$  NMR (75.5 MHz,  $\text{CDCl}_3$ , plus DEPT)  $\delta$  ppm: 20.5 (septet,  $^1J = 19.5$  Hz,  $\text{CD}_3$ ), 55.1 ( $\text{CH}_3$ ), 112.6 (CH), 122.4 (CH), 130.4 (C), 131.4 (C), 134.9 (C), 138.1 (C), 140.0 (C), 158.6 (C). MS (EI),  $m/z$  (%): 951 ( $\text{M}^+$ ).

**sym-Penta(4-methoxy-2,6-dimethylphenyl-3,5- $d_2$ )corannulene (3-( $\text{D}_{Ar}$ )<sub>10</sub>).** The similar procedure to the synthesis of **3** yielded a yellow solid (35%) of **3-(D<sub>Ar</sub>)<sub>10</sub>**: mp  $>350^\circ\text{C}$ . IR (KBr)  $\nu$   $\text{cm}^{-1}$ : 3441, 1589, 1467, 1400, 1310, 1107.  $^1\text{H}$  NMR (75.5 MHz,  $\text{CDCl}_3$ , plus DEPT)  $\delta$  ppm: 1.98 (s, 30H), 3.81 (s, 15H), 7.09 (s, 5H).  $^{13}\text{C}$  NMR (75.5 MHz,  $\text{CDCl}_3$ , plus DEPT)  $\delta$  ppm: 21.3 ( $\text{CH}_3$ ), 55.1 ( $\text{CH}_3$ ), 112.3 (t,  $^1J = 19.1$  Hz, CD), 125.8 (CH), 130.4 (C), 131.4 (C), 134.9 (C), 138.1 (C), 140.0 (C), 158.5 (C). MS (EI),  $m/z$  (%): 931 ( $\text{M}^+$ ).

**Acknowledgment.** This work was supported by the Swiss NFP grant. Dr. Eli Zysman-Colman (University of Zurich) is acknowledged for helpful discussion. We are grateful to Don Truhlar for graciously allowing us to use facilities at the Minnesota Supercomputer Center enabling computations involving the M06-2X functional, which is not yet distributed to the public. We thank Martin Saunders for the latest version of QUIVER.

**Note Added in Proof:** Through discussions with Jack Dunitz, a question has been raised concerning the role of entropy on the kinetic isotope effect. Entropic considerations could stem from low energy librational modes, the higher-order modes of which would become populated with increasing temperature. This could result in the existence of a temperature dependence and a subtle isoselective relationship similar to that found more dramatically for dihalocarbene selectivities, see: Giese, B.; Meister, J. *Angew. Chem. Int. Ed. Engl.* **1978**, *17*, 595.

**Supporting Information Available:** Complete ref 27; the details of the line shape analysis and the crystal structure data of **2**. This material is available free of charge via the Internet at <http://pubs.acs.org>.

JA073052Y